

Interdomain Interactions Modulate Collective Dynamics of the Metal-Binding Domains in the Wilson Disease Protein

Agustina Rodriguez-Granillo,[†] Alejandro Crespo,[‡] and Pernilla Wittung-Stafshede^{*,†,§}

Department of Biochemistry and Cell Biology, Rice University, Houston, Texas 77251, Department of Bioengineering, Rice University, Houston, Texas 77005, and Department of Chemistry, Umeå University, 901 87 Umeå, Sweden

Received: October 1, 2009; Revised Manuscript Received: December 15, 2009

Wilson disease protein or ATP7B is a key player in human copper (Cu) homeostasis. Belonging to the P_{1B} type subfamily of ATPases, its N-terminal region contains six soluble domains (WD1-WD6) connected by linkers that vary in length. These domains share a similar fold and bind Cu(I) in the conserved motif MCXXC. It is unclear why there are six similar domains in the human protein (whereas bacteria and yeast contain only one or two) and why the human metallochaperone Atox1 delivers Cu(I) to only a subset of them. It has been speculated that the extra domains in humans regulate the ATPase in response to different Cu levels, suggesting that, although usually separated by long linkers, the domains can communicate with each other. Here, we performed extensive molecular dynamics simulations on three two-domain constructs in the apo- (WD12, WD34, WD56) and holo- (Cu(I) added to the most C-terminal domain of each construct: WD12c, WD34c and WD56c) forms to investigate how covalent linkage between domains and Cu(I) binding regulate their conformational dynamics. Our results suggest that when linked together the domains do not act as individual units but instead exhibit a distinct pattern of correlated motions, which are domain dependent and modulated by the presence of Cu. Conformational plasticity and degree of reorientation did not correlate with linker length, suggesting strong interdomain communication regardless of the linker length. Our computational findings suggest that cooperativity and long-range communication between domains may be important for the function and regulation of the ATPase.

Introduction

Wilson disease protein or ATP7B belongs to the P_{1B}-type family of ATPases, conserved from unicellular organisms to mammals,¹ which couple ATP hydrolysis to transport copper (Cu) across membranes.^{2–4} ATP7B is a multidomain protein with eight transmembrane domains and several soluble domains.^{5,6} Among the latter, it has six N-terminal metal binding domains (MBDs) termed WDi (where i is the number of the domain 1 to 6, with 1 being the most N terminal domain).^{5,6} The six domains have a similar ferredoxin-like fold ($\beta\alpha\beta\beta\alpha\beta$) and coordinate one Cu(I) via two Cys residues of the conserved motif MXCXXC.^{7,8} The biological reason for the presence of six similar MBDs in humans, as opposed to one or two in bacteria and yeast,¹ is still unclear, as not all of them can interact with the partner Cu chaperone Atox1 in vivo and in vitro.^{9–14} To gain insight into intrinsic molecular differences among individual WD domains, we have previously investigated the conformational dynamics of the individual six WD domains in apo- and holo- (for WD2, WD4, and WD6) forms, via molecular dynamics (MD) simulations.¹⁵ These three holo-domains were selected because they preferably interact with Atox1 (in the case of WD2 and WD4)^{13,14,16} and with WD4 (in the case of WD6).¹³ We found many molecular properties that vary distinctly among the six individual WD domains and could potentially act as selectivity filters to guide Atox1 interactions and interdomain Cu(I) transfer.¹⁵

It has been suggested that interdomain interactions regulate ATP7B function *in vivo*, because of the existence of multiple WDs.¹⁷ These domains are connected by linkers of different length: the longest connects WD4 with WD5, whereas the shortest linker is located between WD5 and WD6. This observation together with the presence of only one or two MBDs in bacterial Cu-ATPases, may lead us to believe that the most N-terminal domains (i.e., WD1–4) behave independently to the most C-terminal domains (i.e., WD56).¹⁷ However, Cu translocation across the membrane by Cu-ATPases appears to be accompanied by profound conformational changes¹⁸ and the entire N-terminal domain of ATP7B can interact specifically with the ATP binding domain in a Cu dependent manner.¹⁹ Moreover, secondary and tertiary structure changes take place in the entire N-terminal domain of ATP7B upon Cu(I) binding.²⁰ This suggests that conformational changes occurring in one MBD, as a consequence of Cu(I) binding for example, may be amplified through the linker regions to a consecutive or more distant MBD, resulting in large-scale conformational changes.¹⁷

Here, we extended our previous computational study on individual domains¹⁵ to explore the effect of domain–domain interactions and/or conformational changes amplified through the linkers among the WDs. We report on MD simulations of the two-domain constructs WD12, WD34, and WD56. We further simulated holo-forms of the same two-domain constructs in which Cu(I) was incorporated into WD2 (WD12c), WD4 (WD34c), or WD6 (WD56c) to study the effect of Cu(I) coordination. Our data suggests that covalent attachment modulates protein dynamics of the individual domains, and that regardless the size of the linker the domains do not behave as

* To whom correspondence should be addressed.

[†] Department of Biochemistry and Cell Biology, Rice University.

[‡] Department of Bioengineering, Rice University.

[§] Department of Chemistry, Umeå University.

beads on a string. Our computational observations are discussed with respect to the possible *in vivo* behaviors of these domains.

Computational Methods

1. Molecular Dynamics Simulations. MD simulations were performed for apo-forms of the two-domain constructs WD12, WD34, and WD56 and in their corresponding Cu-loaded holo-forms with Cu(I) only in WD2, WD4 and WD6 (WD12c, WD34c and WD56c, respectively). These two-domain constructs were selected because there is PDB reported structure for WD34¹⁴ and WD56¹³ only, and because the linker between WD2 and WD3 and between WD4 and WD5 are the longest. The initial structures for the apo-forms correspond to the NMR-reported PDB structures, WD34 (2ROP)¹⁴ and WD56 (2EW9).¹³ Apo-WD12's structure was generated by homology threading calculations with the program Modeler^{21–24} using the structure of the WD56 construct as template (2EW9.pdb, 36% sequence identity), as previously described.¹⁵ For holo-forms of WD12c, WD34c and WD56c, Cu(I) was inserted between the Cys(S) atoms in structures obtained from the MD simulations of the corresponding apo-forms where the S–S distance was lower than 5 Å.

All simulations were performed using Amber9.^{25–28} The initial two-domain constructs were immersed in a pre-equilibrated truncated octahedral cell of TIP3P explicit water molecules²⁹ and counterions were added to neutralize the systems.^{25–28} Protein atoms were described with the parm99SB force field parametrization.³⁰ Parameters of the coordinating Cys and Cu(I) in the holo-forms were taken from ref 15. Briefly, the geometry of holo-WD2, -WD4, and -WD6 were optimized at the QM(PBE/DZP)-MM(Amber99) level (Cu(I) atom plus two methylthiolate groups) followed by HF/6-31G(d)/RESP charge parametrization as described in Amber standard protocol. The protonation state of the titratable residues corresponds to the stable form at pH 7. Water molecules extended at least 12 Å (apo- and holo-forms of WD12 and WD56 and apo-WD34) and 20 Å (holo-WD34) from the surface of the proteins. Simulations were performed in the NPT ensemble (constant pressure of 1 atm and temperature of 300 K was maintained using the Berendsen coupling scheme³¹), employing periodic boundary conditions. A SHAKE algorithm was employed to keep bonds involving hydrogen atoms at their equilibrium length.³² The systems were optimized and equilibrated for 200 ps at 300 K. The structures were then simulated (total run) until the root-mean-square deviation (rmsd) as a function of time of each individual domain was stable for at least 100 ns (production run). Rmsd, rms fluctuations (rmsf) per residue and radius of gyration (Rg) were calculated for each of the systems using the *ptraj* module of Amber9.^{25–28} The cross-correlation matrix of the fluctuations of the Cα atoms from their average values for the production run were calculated for each of the systems using the *ptraj* module of Amber9.^{25–28} Prior to the correlation calculation, the structures in the trajectory were spatially superposed to a common reference structure to exclude all rotational and translational motions exhibited by the molecule in the MD trajectory, as suggested in ref 33.

2. Free Energy Calculations. The interdomain interacting free energy (ΔG) for each two-domain construct was estimated using the *sietraj* program.^{34,35} This program calculates ΔG for snapshot structures from a MD simulation as the sum of the intermolecular van der Waals and Coulomb interactions plus the change in reaction field energy (determined by solving Poisson–Boltzmann equation) and nonpolar solvation energy (proportional to the solvent accessible surface area). ΔG is then scaled by an empirically determined factor.³⁴ The scaling can

TABLE 1: Total Simulation Time (ns), Backbone rmsd (Å) for the Entire Simulation (rmsd_{total}, with Respect to the First Structure) and for the 100 ns of the Production Simulations (rmsd₁₀₀, with Respect to the Average Structure)^a

	time	rmsd _{total}	rmsd ₁₀₀	rmsd ₁₀₀ rel. dev.
WD1.12	239	2.0 ± 0.3	1.4 ± 0.2	14
WD2.12	239	2.3 ± 0.4	1.0 ± 0.2	20
WD1.12c	169	1.8 ± 0.3	0.9 ± 0.2	22
WD2c.12c	169	2.2 ± 0.6	0.8 ± 0.2	25
WD3.34	160	2.4 ± 0.1	1.1 ± 0.1	9
WD4.34	160	2.3 ± 0.6	1.3 ± 0.2	15
WD3.34c	161	1.5 ± 0.3	1.0 ± 0.2	20
WD4c.34c	161	2.4 ± 0.4	1.1 ± 0.3	27
WD5.56	161	2.2 ± 0.1	0.8 ± 0.1	13
WD6.56	161	2.1 ± 0.4	1.3 ± 0.3	23
WD5.56c	159	1.1 ± 0.2	0.9 ± 0.2	22
WD6c.56c	159	2.1 ± 0.7	1.0 ± 0.2	20

^a The relative deviation from the mean value of the rmsd₁₀₀ (rmsd₁₀₀ rel. dev., in %) is also shown.

be considered a crude treatment of entropy-enthalpy compensation, but still contains the caveats of implicit solvation.^{34,36} Here, we estimated ΔG by averaging 1000 calculations from the last 100 ns (production run) of the MD simulations of each two-domain construct. As recommended in the *sietraj* webpage (http://www2.bri.nrc.ca/ccb/pub/sietraj_main.php), the ΔG should be calculated over a stable part of the trajectory. In the case of WD12, WD34c, and WD56c, however, large changes in construct conformation and relative orientations are found in the production simulations. Therefore, the reported values for these constructs correspond to the first 65 and last 35 ns, first 15 and last 85 ns, and the first 30 and last 70 ns, respectively, of the production runs.

Results and Discussion

Although individual domains are similar in size, the two-domain constructs WD12, WD34, and WD56 are very different in size, because of differences in the linker regions. WD1 and WD2 are separated by 12 residues, and the total construct is of 156 residues. The two-domain construct WD56 consists of a total of 149 residues with 6 residues between WD5 and WD6. In the case of WD34, the construct used for NMR¹⁴ consists of additional segments apart from the 27-residue interdomain linker: a N-terminal 17-residue linker (before WD3) and a C-terminal 11-residue linker (after WD4). Therefore, the total size of this construct is 202 residues.

All constructs were simulated for more than 150 ns (Table 1). WD12 was simulated for longer times, because instead of starting from an experimental-determined structure, as in the rest, we started from a built model. Supporting Information Figure S1A shows the rmsd of the entire two-domain constructs (including linkers) as a function of the total simulation time. Upon inspection, we can see that the WD34, which contains the longest linker regions, is the protein with higher deviations, as expected. However, since we are interested in protein dynamics of each individual domain, we simulated until the backbone rmsd of each domain was stable for at least 100 ns (Supporting Information Figure S1B,C).

In the entire simulations, WD3 in the two-domain construct WD34 (WD3.34) and holo-WD4 in the two-domain construct WD34c (WD4c.34c) were the domains that underwent the greatest conformational changes, and the one with highest fluctuations was WD6c in WD56c (WD6c.56c) (Table 1). In the last 100 ns, WD4c.34c exhibited the highest fluctuations, whereas WD3.34 was the one with smallest fluctuations. In any case, all domains have stable rmsd in the production simulation

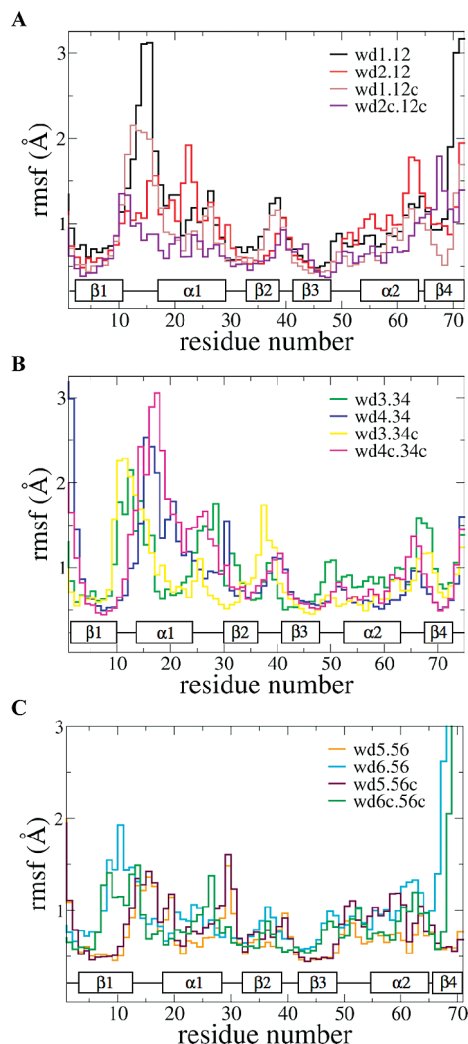


Figure 1. Average fluctuations (rmsf in Å) of backbone heavy atoms (N, C_α, C) per residue (of the production run) for each domain in the apo- and holo-two-domain constructs, WD12 (A), WD34 (B) and WD56 (C). The secondary structure elements are indicated (α_1 , α_2 ; β_1 - β_4), using the first apo-domain as a reference (i.e., WD1, WD3, and WD5). Black, WD1.12; red, WD2.12; brown, WD1.12c; violet, WD2c.12c; light green, WD3.34; blue, WD4.34; yellow, WD3.34c; magenta, WD4c.34c; orange, WD5.56; cyan, WD6.56; maroon, WD5.56c; dark green, WD6c.56c.

time, which suggests that none of them underwent significant conformational changes.

1. Protein Dynamics. 1.1. WD12. As opposed to what we previously observed for the individual domains,¹⁵ backbone fluctuations of WD1 and WD2 in the WD12 construct are not the same; WD1's Cu loop is more flexible than WD2 (Figure 1A). In the case of WD2, Cu-loop fluctuations do not significantly change by the presence of the other domain, although the C-terminus of helix α_1 and the α_2 - β_4 loop are more flexible in the double construct. In particular, the end of helix α_1 loses some secondary structure. On the other hand, the Cu-loop and N-terminus of helix α_1 of WD1 are much more flexible in WD12 than in the isolated domain.¹⁵ As we observed for the individual domains,¹⁵ the N-terminus of helix α_1 loosens up (unwinds) and returns to the original conformation several times during the production time for both domains. Interestingly, Cu(I) binding to WD2 in the WD12c construct not only reduces the overall flexibility of WD2 but also of WD1, maintaining the same tendencies.

The starting model of WD12 was built via homology threading calculations using the structure of WD56 as a model. In WD12's initial structure, whose conformation is maintained for the first ~200 ns of our total simulation, the domains are interacting in a tight unit, and the linker lays between and interacts with the two domains, mediating many of the interactions (Figure 2A). In particular, WD1's helix α_2 and the β_3 - α_2 loop interact with WD2's strands β_1 , β_2 , and β_3 . This interdomain network includes van der Waals (vdW), electrostatic, and hydrogen bond (HB) interactions that include but are not limited to WD1's Gln55, Gln56, and His59 in helix α_2 and WD2's Glu3 in strand β_1 , Arg34 in strand β_2 , and Thr47 in strand β_3 . However, in our production simulation the Rg increases from a mean of 17.3 ± 0.2 Å in the first ~67 ns to a final value of 21 Å (Figure 3). In this final structure, the linker is extended, the interface is weakened (Figure 2A), and both domains are able to move more freely.

To quantify the strength and nature of the domain–domain interacting energy, the free energy (ΔG) and its different contributions were estimated for each of the two-domain constructs (Table 2). Upon inspection, we can clearly see how the interacting energy between WD1 and WD2 significantly weakens from the first 65 ns to the last 35 ns of the production run. In particular, the intermolecular vdW and change in nonpolar solvation energy (proportional to the solvent accessible surface area that becomes buried upon interaction) significantly decreased, which indicates that the domain–domain interface falls apart.

On the other hand, in the holo-form the Rg is constant throughout the production simulation with a mean of 16.6 ± 0.2 Å (Figure 3), indicating that the domains remain in a tight unit interacting with each other. The domain–domain interface, and consequently the interdomain energy, in the holo-form is similar to the one in the apo-form (before they separate, compare ΔG of WD12c to ΔG of WD12 in the first 65 ns, Table 2), although it also covers WD1's strand β_4 (Figure 2B). For example, Glu67 in WD1's strand β_4 makes a strong electrostatic contact with Lys36 in WD2's strand β_2 , which was absent in the apo-form. This additional interaction found in WD12c and not in WD12 is evidenced by an increased of the intermolecular electrostatic energy in the former (Table 2). Glu67 is highly conserved among eukaryotes, often replaced by an Asp, whereas Lys36 is conserved as such in domain 2 of some eukaryotes, including metal-binding domain 2 of the paralog, the Menkes disease protein.¹ Conservation of these residues suggests that this interaction may be important for the function of the protein.

In both apo- and holo-forms, the active sites of both domains remain always facing opposite sides, so that there is no direct interaction between the Cu loops. Also, by looking at the protein structures, we can see that the relative orientation between domains is close to parallel, meaning that both Cu loops point to similar directions (Figure 2), as opposed to an antiparallel conformation, in which one Cu loop would be up and the other one down. As a qualitatively measure of the relative orientation between the domains, we calculated the angle between the domains (or interdomain angle) as a function of the simulation time (Figures 4). The interdomain angle was defined as the dihedral angle between the vectors formed by the backbone heavy atoms of the conserved Met and Pro in the Cu and β_3 - α_2 loops of each domain, respectively. We picked these residues because they are conserved in all six domains and also because they are located in loops that are at opposite ends of each domain (Figure 4A). In the apo-form, although in the first ~67 ns of the production run the two domains are interacting, the relative

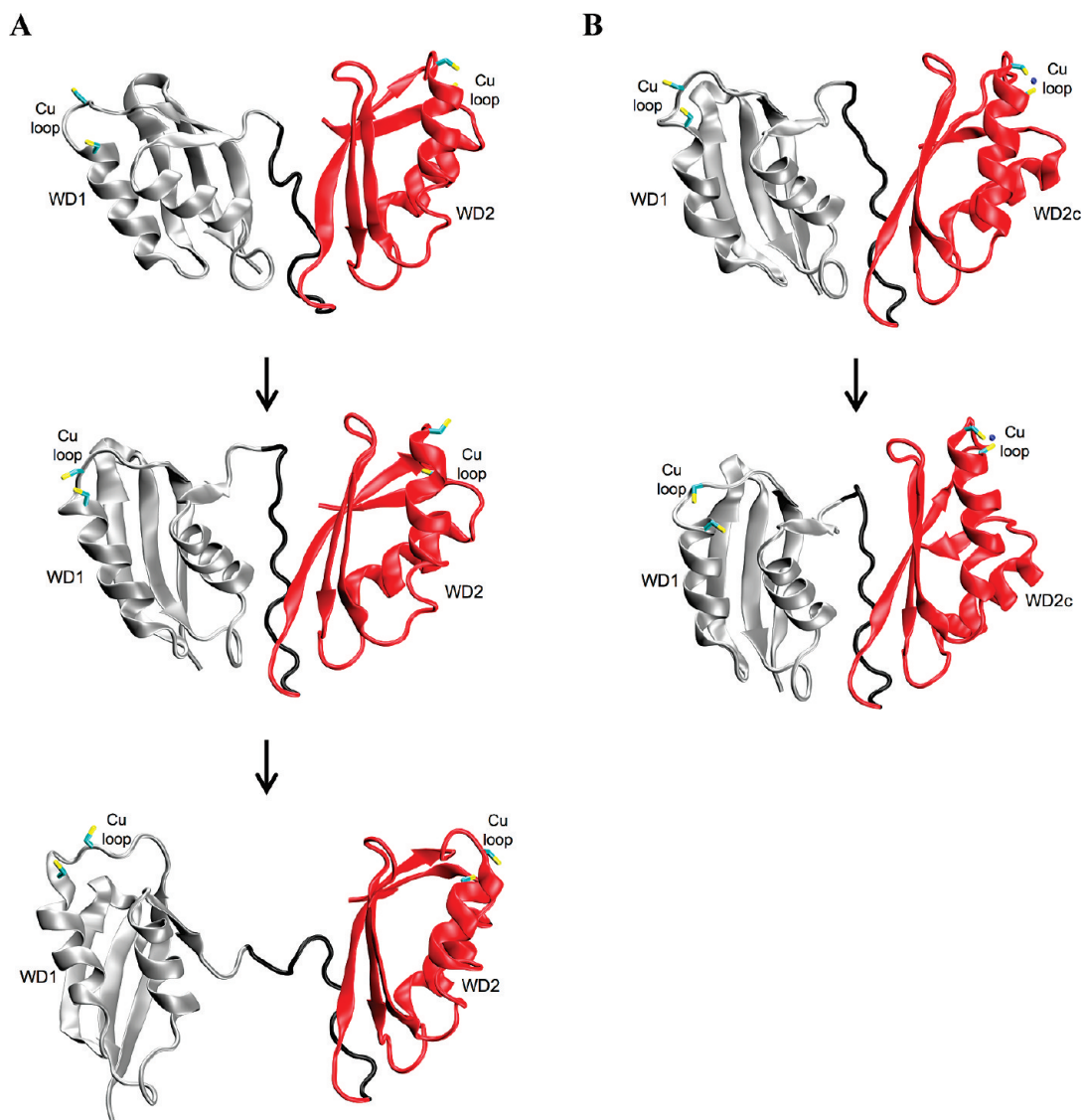


Figure 2. Structure of WD12 from different snapshots of the total MD simulation of apo- (A) and holo- (B) forms. Snapshots are shown in the following order, first, 67.5 ns and last for WD12; and first and last for WD12c. The two Cys residues are shown in sticks.

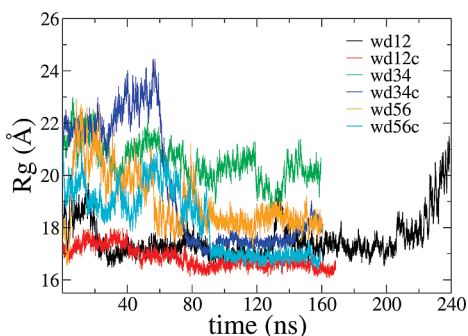


Figure 3. Radius of gyration (R_g in Å) of the backbone heavy atoms (N, C_α , C) of the two-domain constructs (including both individual domains and linker regions) as a function of the total simulation time. Black, WD12; red, WD12c; green, WD34; blue, WD34c; orange, WD56; cyan, WD56c.

orientation between them varies slightly, meaning that the domains are able to rotate with respect to each other (Figure 4B). However, they never reach an antiparallel conformation (Figure 2A). On the other hand, the relative orientation between

WD1 and WD2 is almost fixed in the holo-form (Figure 4B), probably due to their reduced fluctuations.

1.2. WD34. In the case of WD3 and WD4, covalent attachment also affects backbone fluctuations. As a monomer, WD3 behaved in a unique way, because its Cu loop was rigid in comparison with the rest of the protein.¹⁵ In the two-domain construct WD34, WD3's behavior is closer to the rest of the domains (Figure 1B). Its Cu loop is more flexible, whereas helices $\alpha 1$ and $\alpha 2$ and strands $\beta 3$ and $\beta 4$ are less flexible. The generalized reduction in backbone fluctuations in WD3 may be due to interactions of this domain with linker 2 (between WD3 and WD4).

WD4's behavior also changes in the presence of WD3; overall, backbone fluctuations are reduced, except the Cu loop that is more flexible (Figure 1B). Helices $\alpha 1$ and $\alpha 2$ and the $\alpha 2-\beta 4$ loop are less flexible, due to interactions with linker 2. Although helix $\alpha 1$ does not completely unwind and rewind, as previously seen in the individual domain,¹⁵ it loosens up and returns to its original conformation several times. Moreover, the Cu loop adopts a unique conformation, in which both Cys are sticking out from the surface of the protein.

TABLE 2: Domain–Domain Interacting Free Energy (ΔG) of Each Two-Domain Construct in Apo- and Holo-Forms (Calculated for the Production Run), Divided into Nonpolar and Polar Energetic Contributions: Intermolecular van der Waals Interactions (vdW), Change in Nonpolar Solvation Energy (Cavity), Intermolecular Coulomb Interactions (Electrostatic), and Change in Reaction Field Energy (Field)^a

		ΔG	nonpolar contributions		polar contributions	
			vdW	cavity	electrostatic	field
WD12	first 65 ns	-5.6 ± 0.6	-24 ± 5	-3.8 ± 0.7	-48 ± 15	50 ± 14
	last 35 ns	-3.5 ± 0.4	-5 ± 4	-0.6 ± 0.6	-31 ± 18	31 ± 17
WD12c	100 ns	-5.6 ± 0.4	-22 ± 3	-3.6 ± 0.4	-59 ± 14	58 ± 12
WD34	100 ns	-2.8 ± 0.4	-4 ± 3	-0.4 ± 0.6	46 ± 7	-41 ± 6
WD34c	first 15 ns	-4.1 ± 0.6	-16 ± 7	-2 ± 1	53 ± 8	-46 ± 8
	last 85 ns	-7.4 ± 0.7	-45 ± 6	-9 ± 1	20 ± 20	-10 ± 17
WD56	100 ns	-3.7 ± 0.5	-5 ± 3	-0.9 ± 0.6	-20 ± 18	18 ± 15
WD56c	first 30 ns	-3.7 ± 0.3	-4 ± 3	-1.0 ± 0.5	-18 ± 6	16 ± 6
	last 70 ns	-6.1 ± 0.6	-28 ± 5	-5.6 ± 0.9	-15 ± 8	18 ± 7

^a All energy values are in kcal/mol; errors correspond to the standard deviation.

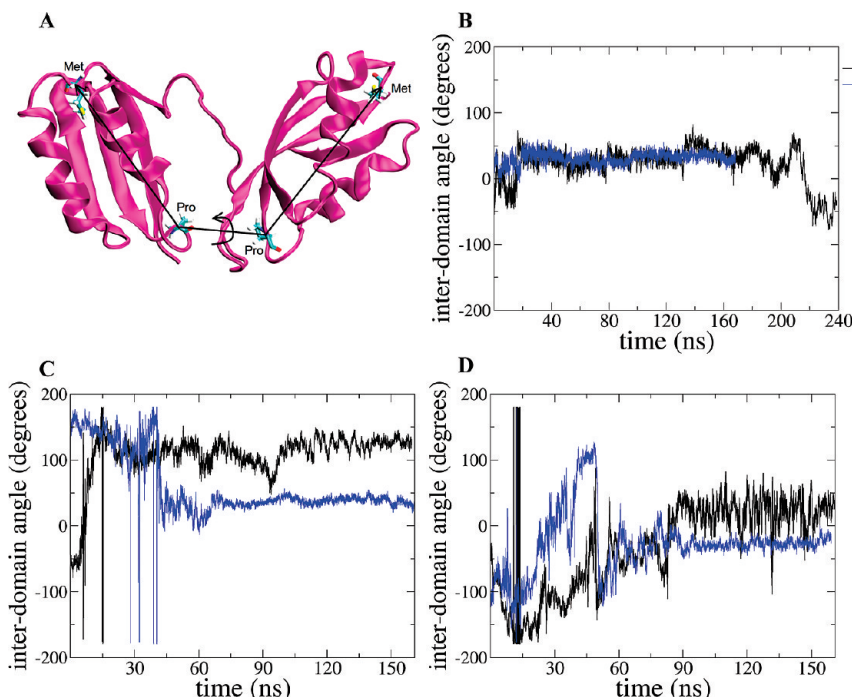


Figure 4. Interdomain angle, defined as the dihedral angle between the vectors formed by the backbone heavy atoms of the conserved Met and Pro in the Cu and $\beta 3$ - $\alpha 2$ loops of each domain, respectively (A), of the two-domain constructs WD12 (B), WD34 (C), and WD56 (D) in apo- (black) and holo- (blue) forms as a function of the total simulation time.

Backbone fluctuations of WD3 are affected by Cu(I) binding to WD4. The $\alpha 1$ - $\beta 2$ and $\beta 3$ - $\alpha 2$ loops, as well as helix $\alpha 2$ and the $\alpha 2$ - $\beta 4$ loop all become less flexible, because these regions interact with WD4 and linker 3 (post WD4) only when Cu(I) is bound to WD4, and this restricts backbone mobility in that area. On the other hand, the $\beta 2$ - $\beta 3$ sheet has greater fluctuations. As opposed to what is seen in the individual domain,¹⁵ WD4 fluctuations increase upon Cu(I) binding in the two-domain construct (Figure 1B). The change is focus on the Cu loop and helices $\alpha 1$ and $\alpha 2$. This holo-domain exhibits significantly higher fluctuations than any of the other two holo-domains, as also observed in the individual domains.¹⁵ Interestingly, the N-terminus of helix $\alpha 1$ unwinds and rewinds several times, which greatly exposes the Cu(I) site, allowing it to protrude out from the surface of the protein, as also observed in the individual domain.¹⁵

The linker between WD3 and WD4 (linker 2) is long enough to possibly allow free motion of both domains, as if they were independent beads on a string. However, this is not necessarily

the case for WD34 in the simulated time. In both apo- and holo-forms, linker 2 interacts extensively with both monomers. These interactions maintain the domains not far from each other, because the linker is not extended. However, there is a drastic difference between the interdomain interacting surface and energy between the apo- and holo-forms during the production simulation (in Figure 5 the last snapshots of both apo- and holo-forms correspond to the conformation adopted during most of the production run). In the apo-form, the interface is weak and the domains do not directly interact between each other, except for some few contacts that include vdW interactions between WD3's $\alpha 1$ - $\beta 2$ loop and WD4's $\beta 3$ - $\alpha 2$ loop. Instead, most of the interactions are mediated by the linker regions (linker 2). This is evidenced by a weak interdomain energy (the weakest among all two-domain constructs, Table 2) with a very poor change in nonpolar solvation energy, indicating that WD3 and WD4 in WD34 are not forming a complex by themselves.

On the other hand, in the holo-form WD3 and WD4 are packed against each other, the interacting surface is extensive

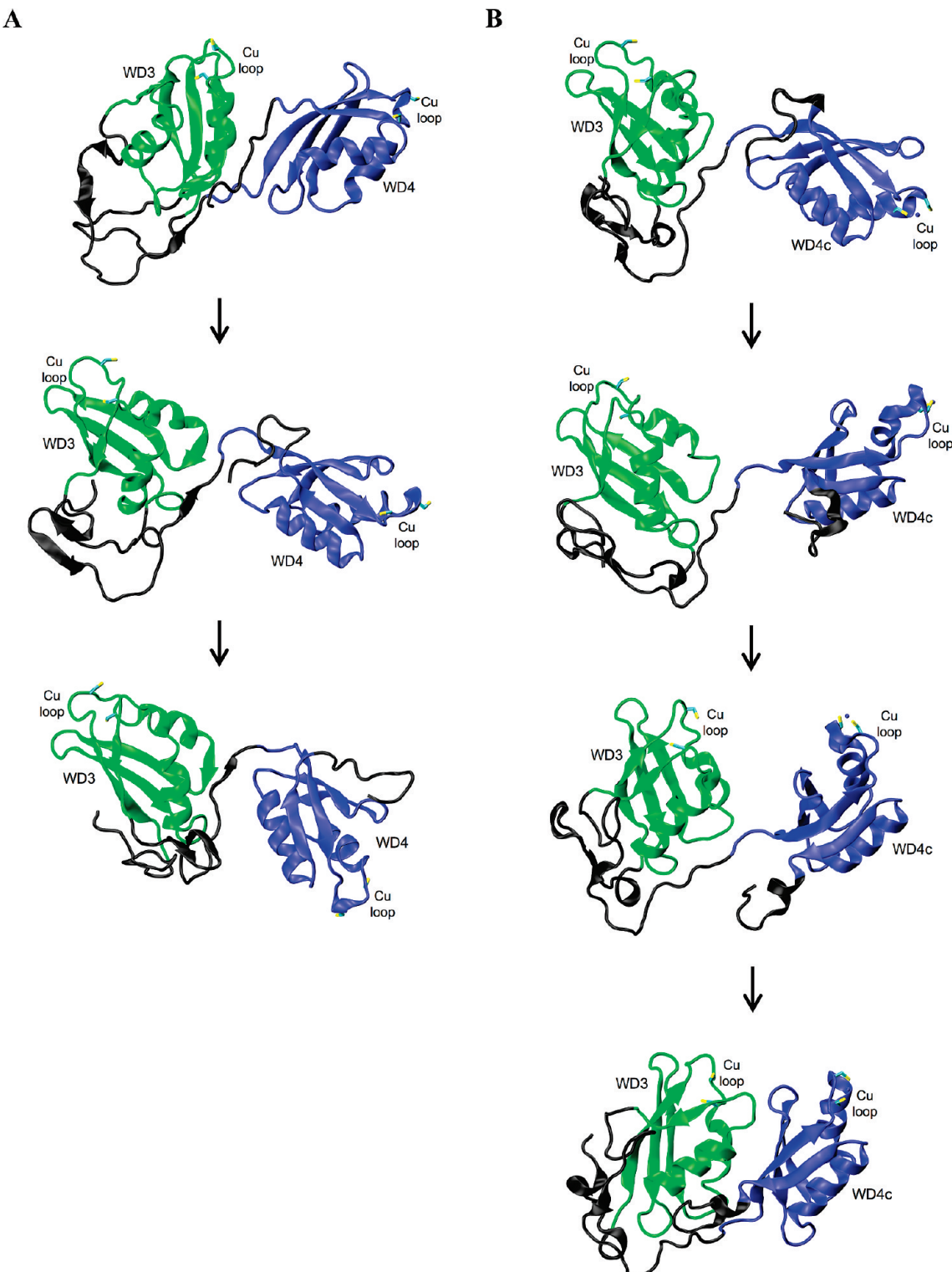


Figure 5. Structure of WD34 from different snapshots of the total MD simulation of apo- (A) and holo- (B) forms. Snapshots are shown in the following order: first, 15 ns and last for WD34; and first, 45 ns, 62 ns and last for WD34c. The two Cys residues are shown in sticks.

and covers a large surface area (the largest among all two-domain constructs, compare the cavity contributions in Table 2), formed by helices α_1 and α_2 from WD3 and the $\beta_1\text{-}\beta_2\text{-}\beta_3$ sheet from WD4, as well as loops and linker regions. This is evidenced by the interacting energy between WD3 and WD4c, which is the strongest among all two-domain constructs (during the last 85 ns of the production simulation), and presents the largest change in nonpolar solvation energy (Table 2), indicating that WD34c forms a compact and stable complex. The interac-

tions involve an intricate network of HB and vdW interactions, which involve WD3's Asn20, Glu23, and Asn24 in helix α_1 and Ala63 and Leu64 in helix α_2 and WD4's Thr6 in strand β_1 , Gln34, Gln35, and Ser37 in strand β_2 , and Thr46 and Leu48 in strand β_3 . Some of these residues are conserved among eukaryotic ATPases or replaced by conservative mutations.¹

In apo-WD34, the Rg varies homogeneously during the simulation, with a mean value of 20.2 ± 0.5 Å in the production run (Figure 3), because although the domains remain at a relative

constant distance, the linker regions are very flexible. Extensive dynamics were also previously observed for the linker regions by NMR.¹⁴ However, the relative orientation of the domains varies along the simulation, meaning that the individual domains are able to reorient between each other, as also previously observed by NMR.¹⁴ Initially, their orientation is close to being parallel (Figures 5A). However, between the first 4 and 15 ns of the total simulation, their arrangement changes (they rotate) and they adopt an antiparallel conformation (Figures 4C and 5A). Although an overall antiparallel arrangement is maintained in the rest of the simulation, the domains are still able to freely rotate between each other (Figure 4C).

In the holo-form, the Rg is initially close to the one in the apo-form with a mean value of 19.7 ± 0.8 Å in the first 10 ns of the production run, after which the domains collapse against each other, to reach a mean value of 17.6 ± 0.3 Å in the last 90 ns (Figure 3). In this conformation, WD3 and WD4 remain in a tight and compact unit, interacting between each other and with the linker regions (Figure 5B). In this case, in the initial structure the domains are in an extended and antiparallel orientation (Figure 5B), in which they are able to rotate between each other (Figure 4C). However, they finally rotate to adopt a parallel orientation, prior to the collapse, in which they remain for the rest of the simulation (Figures 4C and 5B). In any case, the active sites of each domain are far away and never face each other.

1.3. WD56. Previously, we found that WD5 exhibits increased conformational flexibility as an individual domain,¹⁵ and helix α 1 was very disordered and distorted. On the other hand, the entire backbone flexibility of WD5 is significantly reduced in the two-domain construct (Figure 1C). In particular, the Cu loop and helix α 1 are more structured. We also found that WD6 was the most rigid of all individual six domains.¹⁵ In the two-domain construct, however, WD6 is more flexible, and it is now WD5 the most rigid one. As an individual domain, only a subtle movement of the N-terminus of helix α 1 in WD6 could be observed.¹⁵ In the two-domain construct this unwinding/rewinding is intensified. When Cu(I) is bound to WD6 in WD56c, the C- and N-terminus of helices α 1 and α 2 in WD5, respectively, become more flexible. These regions define an interface at the surface of the protein, which may be important for partner interactions in the cell. On the other hand, WD6's flexibility is reduced upon Cu(I) binding in the two-domain construct. However, the individual holo-domain¹⁵ is much more rigid than holo-WD6 in WD56c.

In the initial (NMR¹³) structure of apo-WD56, both domains are in a tight unit interacting between each other (Rg of 17.5 Å) and their orientation is parallel (Figure 6A). However, when the simulation starts, WD5 and WD6 separate (after ~ 4 ns), evidenced by an increase in the Rg up to ~ 23 Å (Figure 3) and an extension of the linker that separates them (Figure 6A). After ~ 55 ns, the domains come closer again and remain together during the production run (Rg of 18.4 ± 0.5 Å, Figure 3); however, they adopt a more extensive conformation than the initial one, because of a different conformation of the linker. In particular, the interacting energy for these domains is relatively weak, comparable for example to the one between WD1 and WD2 at the end of the simulation (after they separate) (Table 2). The conformational change takes place in two steps. First the domains separate (see Rg plot at ~ 4 ns, Figure 3) and rotate so that now their orientation is such that they are antiparallel (note how the interdomain angle smoothly starts to increase in magnitude at ~ 4 ns until it approaches ~ 180 degrees at ~ 12 ns, Figure 4D and Figure 6A). Finally, they rotate again to the

initial orientation (after it reaches ~ 180 degrees, the interdomain angle smoothly starts to become closer to zero again, Figure 4D) and come closer together (see Rg plot at ~ 55 ns, Figure 3 and Figure 6A). Although some variation in the interdomain angle suggests that the construct is not rigid, during the production run, WD5 and WD6 remain in a similar relative orientation (Figure 4D). This is consistent with the rotational correlation time of the two-domain construct being twice the one for a monomer in NMR experiments.¹³

The final conformation adopted by WD5 and WD6 in the apo-form is different to the one observed in the initial (NMR) structure,¹³ although both conformations likely represent minima in the phase space of the system. In the initial structure, WD6's strands β 1, β 2, and β 3 are facing WD5's helix α 2 and strand β 4 (Figure 6A). During our simulations, the domains flipped, so that now WD5's strands β 1, β 3, and β 4 interact with residues in WD6's N-terminus of strand β 1 and helix α 2 and C-terminus of strand β 4. The interactions involve a network of vdW, electrostatic, and HB interactions; the most stable is between WD6's Arg53 at the N-terminus of helix α 2 with WD5's Phe7 in strand β 1 and Glu45 in strand β 3, which are pretty conserved residues among the corresponding domains in eukaryotes.¹ Arg53 in WD6 aligns with Gln55 in WD1, pointing to a similar conformation in which these domains interact in the two-domain constructs. Most importantly, mutation of Arg53 to a Trp³⁷ or a Gln^{38,39} results in Wilson disease. These changes will likely disrupt a strong salt bridge between WD5's Glu45 and WD6's Arg53 that may be relevant in vivo. In the NMR structure, Arg53 is pointing to the solvent and makes no contacts with residues in WD5.¹³ The fact that Arg53 is mutated in Wilson disease patients supports the relevance of the WD56 conformation observed in our MD simulations.

On the other hand, in the holo-form WD5 and WD6 are initially further apart with a Rg of 19.2 ± 0.7 Å in the first ~ 30 ns of the production run, after which they collapse into a tight unit with a Rg of 16.9 ± 0.2 Å in the last ~ 70 ns (Figures 3 and 6B). In this case, the domains are able to slightly move between each other only in the first ~ 30 ns of the production run (Figure 4D), similarly to the apo-form. The similarity between the behavior of WD56 and the first ~ 30 ns (of the production run) of WD56c is also evidenced by a similar interacting energy (Table 2). However, after the first ~ 30 ns WD5 and WD6c remain in a fixed orientation in which they interact extensively (Table 2). The conformation adopted by the domains is similar to the one in the apo-form (the nature of the interactions found in the apo-form are conserved in the holo-form, although the strength significantly changes, Table 2). This points to the importance of Arg53 in mediating protein–protein interactions also in the presence of Cu(I). However, these domains are more tightly packed against each other in the holo-form (Table 2, compare the change in nonpolar solvation energy between WD56 and WD56c), and therefore the interacting surface covers a bigger surface area (Figure 6B), including WD5's strand β 2 and the β 2– β 3 loop and WD6's entire helix α 2, the α 2– β 4 loop, and strand β 4. This interdomain surface is very stable, thanks to an extensive network of vdW, electrostatic, and HB interactions, which maintain the domains very close to each other, as part of a functional unit.

2. Cross-Correlated Motions. To gain insight into the cooperative dynamics and long-range communication between individual domains in the two-domain constructs, as well as the effect of Cu(I) binding, the cross-correlation matrix⁴⁰ for the C α atoms was calculated for all protein forms (see Figure 7 for two-domain constructs and Supporting Information, Figure

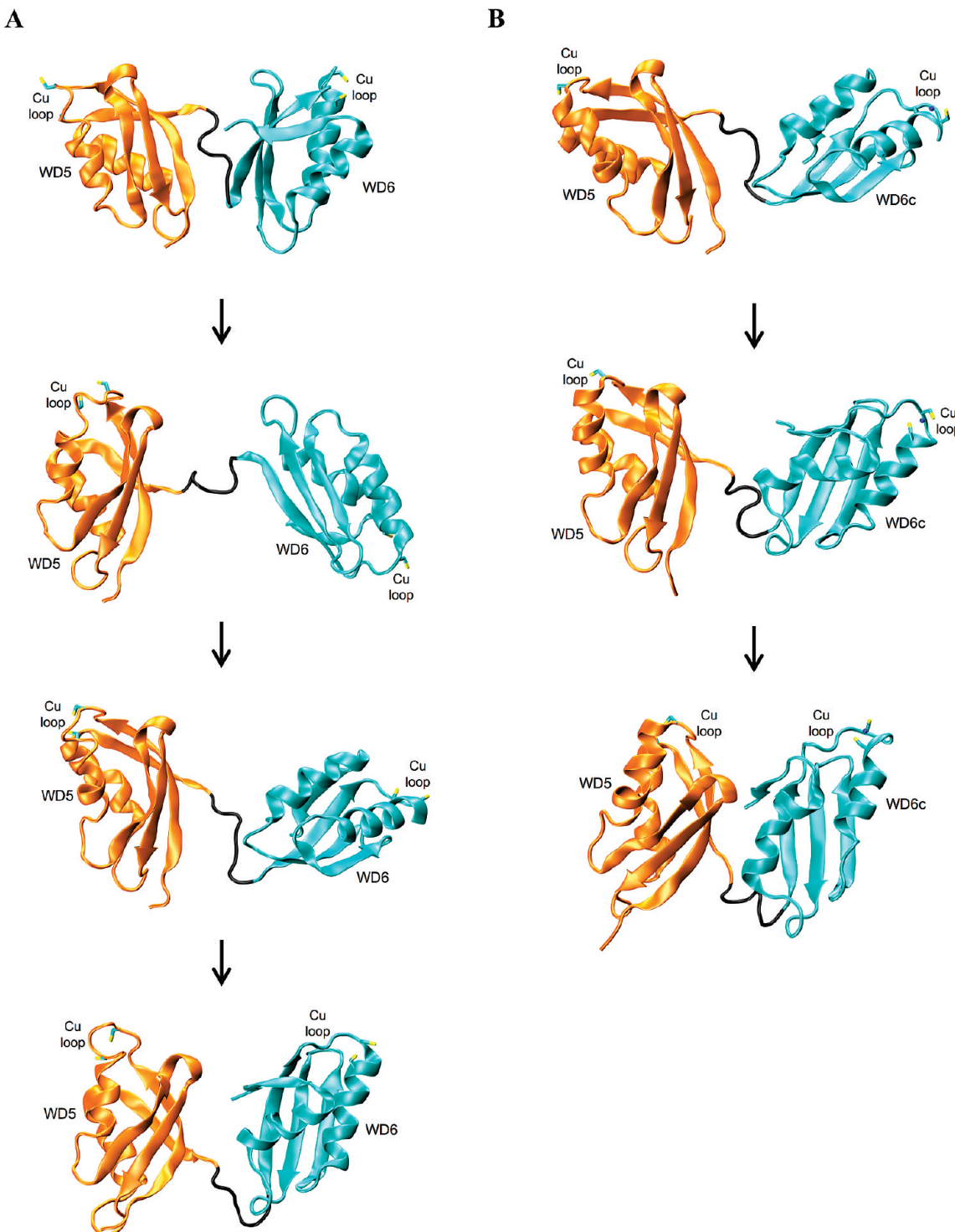


Figure 6. Structure of WD56 from different snapshots of the total MD simulation of apo- (A) and holo- (B) forms. Snapshots are shown in the following order: first, 12 ns, 30 ns, and last for WD56; and first, 30 ns and last for WD56c. The two Cys residues are shown in sticks.

S2 for individual domains). In this analysis, positive or in-phase correlations are indicated in red (strong) and yellow (moderate), and negative or out-of-phase correlations are indicated in black (strong) and cyan (moderate).

2.1. Intradomain Correlations. In all cases, we find only moderate cross-correlated regions in the individual proteins (Supporting Information, Figure S2), except for the diagonal that corresponds to the correlation of a residue with itself. On the other hand, correlations of the three two-domain constructs show that both domains are strongly correlated and the presence of the other

domain significantly enhances both in-phase and out-of-phase correlations within each individual domain (intradomain correlations) (Figure 7). This suggests that presence of the other domain is needed to induce specific motions within each individual domain. This also agrees with previous simulations of multidomain proteins in which intradomain correlations were also significantly weaker in the individual domains.^{41,42} All six domains present an overall similar correlation pattern, which is expected since all have similar fold and overall similar dynamics (e.g., in all cases the Cu loop is the most flexible region).

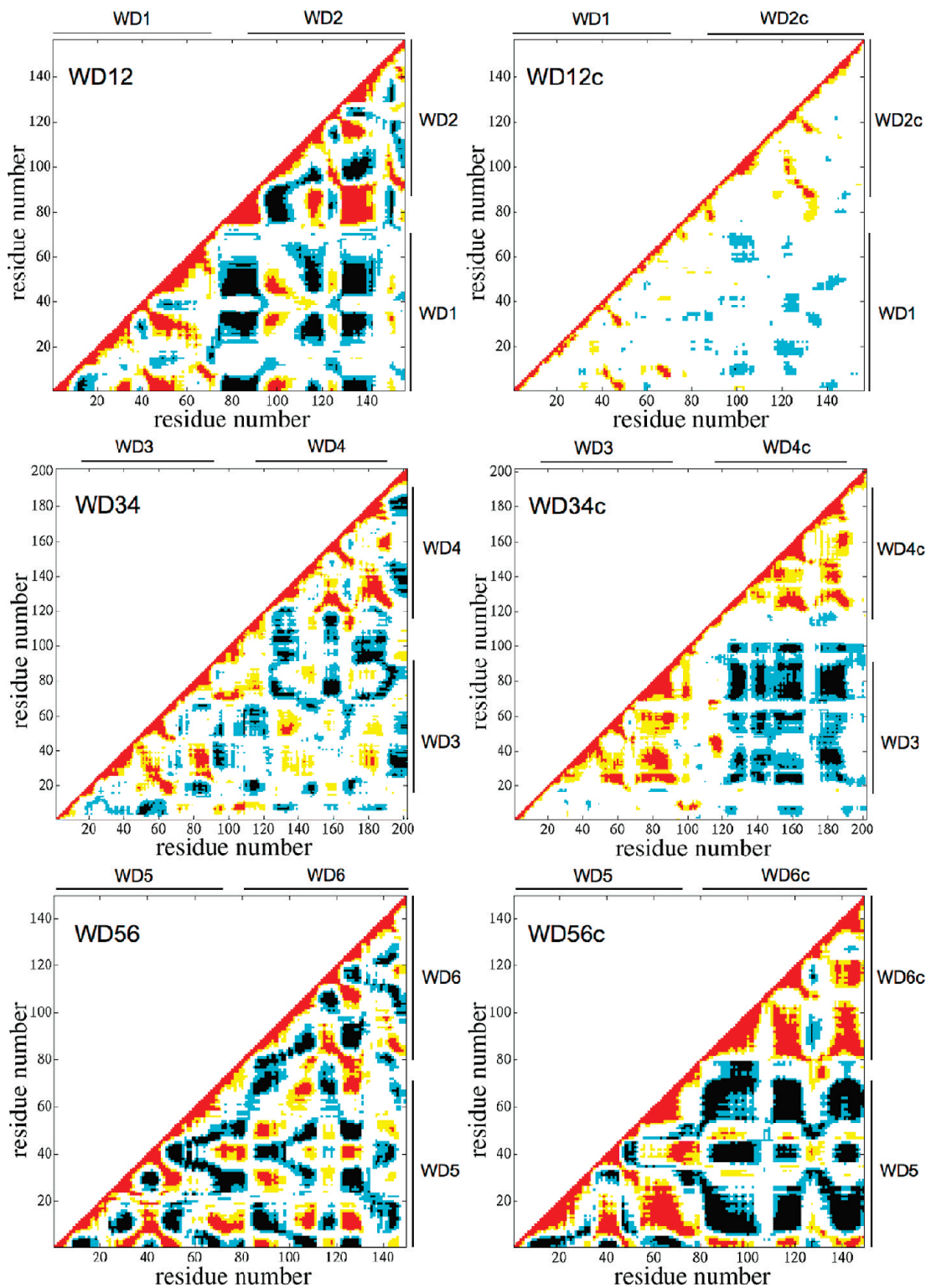


Figure 7. Cross-correlation matrices of fluctuations of $\text{C}\alpha$ atoms from their average values during the production simulation for WD12, WD12c, WD34, WD34c, WD56, and WD56c. The degree of correlation is color-coded: red, strong positive ($0.6 \leq C_{ij} \leq 1$); yellow, moderate positive ($0.4 \leq C_{ij} < 0.6$); black, strong negative ($-0.6 \leq C_{ij} \leq -1$); cyan, moderate negative ($-0.4 \leq |C_{ij}| < 0.6$); white, weak or no correlation ($-0.4 < C_{ij} < 0.4$). The limits of each domain are indicated.

In all cases, positive correlation is observed between residues forming secondary structure elements, which hold the fold together: helices $\alpha 1$ and $\alpha 2$; sheets $\beta 1\text{-}\beta 3$, $\beta 2\text{-}\beta 3$, and $\beta 1\text{-}\beta 4$; helix $\alpha 1$ with strand $\beta 2$; strand $\beta 1$ with helix $\alpha 2$, strand $\beta 3$ and helix $\alpha 2$ with strand $\beta 4$. In-phase motions are also found between loops and secondary structure elements: Cu loop with

helix $\alpha 1$; strand $\beta 1$ with $\alpha 1\text{-}\beta 2$ and $\beta 2\text{-}\beta 3$ loops; $\alpha 1\text{-}\beta 2$ loop with $\beta 3\text{-}\alpha 2$ loop; and Cu loop with $\alpha 2\text{-}\beta 4$ loop.

On the other hand, negative correlations are observed between residues in the Cu loop and helix $\alpha 1$ and residues distant in both sequence and tertiary structure, including the $\beta 3\text{-}\alpha 2$ loop and strand $\beta 4$. Similarly, the $\alpha 2\text{-}\beta 4$ loop presents out-of-phase

motions with distant residues including strand $\beta 1$ and the $\beta 3$ - $\alpha 2$ loop. Besides the Cu loop, the $\alpha 2$ - $\beta 4$ loop may also have functional relevance since a conserved Phe residue is located here, and this loop is believed to form part of the metallochaperone-target interaction interface.^{13,14,43,44} This Phe aligns with conserved residues in eukaryotic and prokaryotic metallochaperones that appear to have an important role in Cu chaperone structure and dynamics.^{45–47} These concerted motions, therefore, may altogether help modulate the flexibility of two key loops in these domains.

Cu(I) coordination to WD2, WD4 and WD6 in the two-domain constructs not only changes the correlation pattern within the holo-domain, but also within the consecutive apo-domain (Figure 7). In all cases, intradomain out-of-phase motions are reduced or absent. However, WD5 and WD6 in WD56c still present significant negative correlations.

2.2. Interdomain Correlations. In all three constructs, interdomain correlations are significant and involve both residues that are close to each other, which form the domain–domain interacting interface and residues that are distant both in sequence and space. This coupling between domains, which is possible because of the linker regions that connect them, emphasize a long-range domain–domain interaction that might be important for the function and regulation of ATP7B in vivo.

Some similarities are found between interdomain correlations in WD12, WD34, and WD56 (Figure 7). In all cases, Cu(I) binding to one domain significantly affects the interdomain collective motions. Whereas in the apo-form we found both in-phase and out-of-phase correlations, upon Cu(I) binding interdomain correlations are only or mainly negative. These changes may provide individual domains a way to “communicate” among each other. For example, Cu(I) binding to one domain may alter the interplay between the consecutive domain, which at the same time may affect the tertiary structure of the full-length N-terminal domain, as previously observed experimentally.²⁰ This conformational change of the entire N-terminal domain may be crucial for the ATPase regulation in vivo.²⁰

Interestingly, many of the interdomain motions, both in the apo- and holo-forms, involve the Cu loop, helix $\alpha 1$, and the $\alpha 2$ - $\beta 4$ loop of each domain with each other and several other distant residues located in the other domain. These shared collective movements may be functionally important, since all these regions contain conserved residues with functional relevance (e.g., for interaction with the metallochaperone). In the apo-forms, the type of correlation involving these residues varies among the two-domain constructs. In the holo-form, however, both the Cu (including the two Cys residues) and $\alpha 2$ - $\beta 4$ (including the conserved Phe) loops are anticorrelated between each other. Moreover, some regions are similarly correlated in all constructs. For example, in the apo-forms, the C-terminus of helix $\alpha 1$, the $\alpha 1$ - $\beta 2$ loop, and N-terminus of strand $\beta 2$ of each domain are always positively correlated with the C-terminus of strand $\beta 1$, the Cu loop, and the N-terminus of helix $\alpha 1$.

2.2.1. WD12. In WD12, the linker region and beginning of WD2's $\beta 1$ strand is strongly anticorrelated with several residues in WD1, including strands $\beta 1$, $\beta 2$ and $\beta 3$; helices $\alpha 1$ and $\alpha 2$; and the $\alpha 1$ - $\beta 2$ and $\beta 3$ - $\alpha 2$ loops. Some of these regions define the domain–domain interface during the first ~ 67 ns of the production simulation (after which the interface weakens). Interestingly, WD1's Cu loop is negatively correlated with residues in WD2 and the opposite is true for WD2's Cu loop; however, both Cu loops are negatively correlated.

Although in WD12c the individual domains make more contacts than in the apo-form, interdomain correlations are weaker than in WD12, probably because backbone fluctuations are significantly reduced upon Cu(I) binding. Only few interdomain out-of-phase motions are found in WD12c, and these include residues that are close between each other in space and are part of the domain–domain interface: WD1's N-terminus of helix $\alpha 2$ with the linker and WD2's N-terminus of strand $\beta 1$; and the linker with both WD1's strand $\beta 4$ and WD2's strand $\beta 1$. Although the domains are in close contact, the decreased in overall flexibility may account for the weaker correlations found in the presence of Cu(I). However, both Cu loops are still flexible, especially WD1's Cu loop, which may explain why the majority of the out-of-phase movements involve these regions.

2.2.2. WD34. In WD34, correlations are weaker to the ones found in WD12. This may be due to the fact that the linker between WD1 and WD2 is much shorter than the one between WD3 and WD4, so domain–domain correlations are more easily propagated through a shorter linker. As mentioned before, in apo-WD34 the domain–domain interface is small. Cross-correlations are found between residues that interact directly and between nearby regions. In-phase correlations are found between residues forming the interacting interface, which include WD3's C-terminus of helix $\alpha 2$ and the $\alpha 2$ - $\beta 4$ loop with WD4's $\beta 3$ - $\alpha 2$ loop. On the other hand, out-of-phase movements are found between WD3's $\alpha 1$ - $\beta 2$ loop and the same region in WD4; WD3's $\alpha 1$ - $\beta 2$ loop, strand $\beta 2$ and $\beta 2$ - $\beta 3$ loop and WD4's strand $\beta 3$ and $\beta 3$ - $\alpha 2$ loop; WD3's strand $\beta 3$ and $\beta 3$ - $\alpha 2$ loop and the same residues in WD4; and between WD3's $\beta 3$ - $\alpha 2$ loop and N-terminus of helix $\alpha 2$ and WD4's $\beta 3$ - $\alpha 2$ loop, helix $\alpha 2$, $\alpha 2$ - $\beta 4$ loop and strand $\beta 4$. Moreover, as opposed to in WD12, we found the Cu loop and helix $\alpha 1$ of each domain to be positively correlated.

As opposed to WD12c, correlations are accentuated upon Cu(I) binding to WD34c. This may be explained by two reasons. First, the interacting interface between WD3 and WD4 significantly increases upon Cu(I) binding, whereas it increases to a lesser extent in WD12c. Second, the backbone fluctuations of WD3 and WD4c are much larger than those of WD1 and WD2c. To recall, WD4c in WD34c was found to be the most flexible holo-domain. In fact, WD4c fluctuations increased upon Cu(I) binding, instead of decreasing as in the rest of the domains. For these reasons, interdomain correlations are strong and negative. Many of these correlations involve residues forming or near the interface between the two domains: WD3's helices $\alpha 1$ and $\alpha 2$, strand $\beta 4$ and the Cu and $\alpha 2$ - $\beta 4$ loops with WD4's strands $\beta 1$, $\beta 2$, $\beta 3$, the Cu and $\beta 2$ - $\beta 3$ loops; WD3's helix $\alpha 2$, $\alpha 2$ - $\beta 4$ loop and strand $\beta 4$ with WD4's strands $\beta 1$ and $\beta 4$, helix $\alpha 2$ and the Cu and $\alpha 2$ - $\beta 4$ loops. This strong negative coupling between the motion of WD3 and WD4c may be relevant from a functional point of view, for example, to promote interdomain Cu(I) transfer from WD4c to a more C-terminal domain (e.g., WD6).

2.2.3. WD56. Interdomain correlations in WD56 are similar to the ones found in WD12. This may be because the linker between WD5 and WD6 is comparable in length to the one in WD12. Therefore, correlations are strong instead of moderate as found in WD34, probably because backbone motions can be more easily propagated through a shorter linker. However, despite the short linker that separates them, the interacting interface between WD5 and WD6 is relatively small. The motion of residues near the domain–domain interface is negatively coupled, that is, WD5's N-terminus of strand $\beta 1$ with WD6's

C-terminus of strand β 3 and the β 3- α 2 loop. As in WD12, the motion of the Cu loop and N-terminus of helix α 1 of each domain is positively correlated.

The effect of Cu(I) binding to WD56c is similar to the one found in WD34c: Cu(I) binding intensifies the degree of cross-correlations motions instead of decreasing it, as in WD12c. The reasoning is similar to the one for WD34: WD56c interacting surface is extensive and the flexibility of WD56 upon Cu(I) binding is not reduced as in WD12c. Negative interdomain correlations are found between residues that form or are near the domain–domain interface, that is, WD5’s strand β 1, Cu loop, helix α 1 and α 1- β 2 loop with WD6’s strands β 1 and β 4, helices α 1 and α 2, Cu and α 2- β 4 loops; WD6’s helix α 2, α 2- β 4 loop and strand β 4 with WD5’s strand β 4, helix α 2 and β 2- β 3, β 3- α 2 and α 2- β 4 loops; WD5’s C-terminus of strand β 3, β 3- α 2 loop and N-terminus of helix α 2 with the same residues in WD6. Again, as suggested for WD34c, this strong interplay between WD5 and WD6c found only in the holo-form may be key to promote Cu(I) transfer to the transmembrane sites of ATP7B.

Conclusions

We have explored the conformational dynamics of the six WDs of ATP7B as pairs (WD12, WD34, and WD56) with and without one Cu(I) added to each pair to shed light into interdomain interactions that may regulate Cu transport. In all cases, protein dynamics significantly changed when each domain was covalently linked to its consecutive domain, in comparison to the individual domains.¹⁵ Moreover, Cu(I) binding to one domain modulated not only the behavior of that same domain, but also the one of the apo-domain that was covalently linked to. This suggests that structure and dynamic changes occurring in one domain upon Cu(I) binding are being translated or propagated to the next domain through the linker as a way of “communicating” between each other. This “communication” is possible because of the presence of interdomain correlations. Interestingly, Cu(I) binding to one domain induced not only changes in the individual domains, but also tertiary structure rearrangements of the entire construct. Secondary and tertiary structure changes were also observed experimentally upon Cu(I) binding to the entire N-terminal domain of ATP7B.^{20,48} In particular, in all our MD simulations, Cu(I) binding induced a more compact tertiary structure, in which the domains interact more stably and with a larger interacting surface area. This is in agreement with a “structural tightening” observed *in vitro* upon Cu(I) binding to the N-terminus domain of ATP7B.⁴⁹ Moreover, the transition between apo- and holo-forms was further accompanied by conformational changes of the linker regions. This observation is consistent with the limited proteolytic digestion pattern of the N-terminal domain being affected by the presence of Cu.^{12,49} These conformational changes upon Cu(I) binding amplified by linkers may alter the overall arrangement of the domains in the full-length N-terminal domain, which may be important for the function and regulation of the protein *in vivo*.¹⁷ For example, there is evidence that the N-terminal domain of ATP7B is able to interact with the ATP-binding domain but only in the absence of Cu.¹⁹ Conformational changes of the entire N-terminal domain upon Cu(I) binding, similar to the ones observed here in the two-domain constructs, may reverse its interaction with the ATP-binding domain and trigger Cu(I) transport across the membrane. Additionally, these conformational changes may trigger ATP7B translocation from the Golgi membrane to a vesicular compartment when Cu levels are elevated.^{50,51}

Whereas Cu(I) binding to WD12 weakened the interdomain correlations, the opposite was true for Cu(I) binding to WD34 and WD56. This difference in the coupling between the domains may highlight different individual functions of these proteins in the context of the entire ATPase. For example, strong anticorrelations between WD3-WD4 and WD5-WD6 upon Cu(I) binding to WD4 and WD6, respectively, may promote vectorial Cu(I) transfer to WD6¹³ and the transmembrane Cu sites,¹⁷ respectively.

Interestingly, the interacting surface in all domains covered similar protein regions. In all our apo- and holo-two-domain constructs the Cu loops of each domain remain at opposite sides and far from each other. This suggests that interdomain Cu(I) transfer between these consecutive domains (e.g., from WD2c to WD1, WD4c to WD3, or from WD6c to WD5) is not likely to occur. Instead, it is more likely that interdomain Cu(I) transfer will occur between domains that are further apart, for example, between WD2 and WD4 and between WD4 and WD6. Although the linker between WD3 and WD4 is long enough to allow domain rearrangements that may allow interdomain Cu(I) transfer, Cu loops were never close enough to suggest this as a possibility.

In a recent study based on 6 ns MD simulations of two-domain metal-binding domain constructs from different organisms, it was proposed that each domain exhibited increasing freedom of reorientation and weaker interacting energy with increasing linker length.⁵² However, based on more than 150 ns of MD simulation for three different two-domain constructs, our results suggest that the interplay between linker length, interacting energy and conformational freedom is less trivial. For example, even though the linker between WD1 and WD2 is two times longer than the one between WD5 and WD6, individual domains were able to reorient more freely in WD56 than in WD12 with respect to the initial structures. Starting from a parallel orientation, whereas WD56 was able to adopt an antiparallel orientation to finally return to the original conformation in 55 ns, individual domains in WD12 were unable to reach such orientation in 239 ns. Also, the interacting energy between WD1 and WD2 (during the first ~65 ns of the production run) was stronger than the one between WD5 and WD6 in the apo-forms. Moreover, Cu(I) binding can significantly alter the relationship between linker length and interacting energy. For example, because apo-WD34 has the weakest interdomain energy, one might conclude that this is due to the long interdomain linker. However, this may not be the case, since WD34c exhibited the strongest interdomain energy.

On the other hand, previous NMR experiments on the same WD34 construct suggested that these domains behave independently from each other, as beads on a string.¹⁴ Although we observe the domains not to be completely independent, since their motion is coupled by a linker that connects them, they are free to reorient with respect to each other in the entire simulation of the apo-form and in some portion of the simulation of the holo-form. This independent tumbling between domains agrees with the NMR data.¹⁴ Similar NMR experiments on the same construct revealed that holo-Atox1 is only able to form a stable Cu-dependent adduct with WD4, although Cu is transferred efficiently to both domains.¹⁴ Two possibilities could explain this observation, Atox1-Cu-WD3 adduct is too weak for NMR detection or, once WD4 receives Cu from Atox1, Cu is transferred intermolecularly to WD3.¹⁴ Because at no time during our simulations were WD3’s and WD4’s active site close enough to allow interactions, we propose the first scenario as more likely to occur. We propose two reasons as to why Atox1-

Cu-WD3 adduct was not detected by NMR. First, WD4's Cu loop and helix α 1 are more flexible than WD3's, and this may facilitate interactions with the metallochaperone. Second, WD4 is more accessible than WD3 within the two-domain construct, which may increase the probability of interactions between WD4 and Atox1. Whereas WD3 interacts with the linker regions and its Cu loop faces most of the time the domain–domain interface, WD4's Cu loop is always facing the surface. These differences observed between WD3 and WD4 may result in a more transient and less stable complex between Atox1 and WD3.

Because of the longest and shortest linker separating WD4 from WD5, and WD5 from WD6, respectively, and based on the WD56 NMR solution structure, it has been proposed that these two last domains behave as a functional and compact unit.¹³ A recent 6 ns MD simulation on the same construct showed that WD56 also remain in a tight unit.⁵² Because WD6 is the most C-terminal domain, that is, closest to the membrane (and because bacterial ATPases contain only one or two metal-binding domains), it has been proposed to be the one that, after picking up Cu from other domain, for example, WD4¹³ or from Atox1,¹⁶ delivers Cu to the transmembrane sites for subsequent Cu translocation.¹⁷ It is tempting to speculate that in order to perform the aforementioned tasks, WD56 may still need to have certain degree of conformational plasticity, rather than remaining as a tight and rigid structure. Here, thanks to our extensive simulation time, which allowed us to explore a vast range of conformational space, we can conclude that, although WD56 remains in a close conformation in most of the production simulation time, the individual domains still have enough conformational flexibility to allow for movements with respect to each other, suggesting that they do not behave as a rigid entity.

Taken together, our in silico results provide new insights into how the MBDs in ATP7B interact with each other with direct implications for their Cu transfer activity *in vivo*.

Abbreviations

Cu, copper; MBD, metal binding domain; WD, Wilson disease protein MBD; MD, molecular dynamics; rmsd, root-mean-square deviation; Rg, radius of gyration; rmsf, root-mean-square fluctuations; vdW, van der Waals; HB, hydrogen bond.

Acknowledgment. We thank Drs. Bertini and Banci for providing the PDB structure of WD34 before being deposited in the PDB. Part of this work was supported by the Rice Computational Research Cluster (NSF Grant CNS-0421109), by a partnership between Rice University, AMD, and Cray, by the Shared University Grid at Rice (NSF under Grant EIA-0216467), and by a partnership between Rice University, Sun Microsystems, and Sigma Solutions, Inc.

Supporting Information Available: Figures S1 and S2. This material is available free of charge via the Internet at <http://pubs.acs.org>.

References and Notes

- Arnesano, F.; Banci, L.; Bertini, I.; Ciofi-Baffoni, S.; Molteni, E.; Huffman, D. L.; O'Halloran, T. V. *Genome Res.* **2002**, *12*, 255.
- Pufahl, R. A.; Singer, C. P.; Pearson, K. L.; Lin, S. J.; Schmidt, P. J.; Fahrni, C. J.; Culotta, V. C.; Penner-Hahn, J. E.; O'Halloran, T. V. *Science* **1997**, *278*, 853.
- Klomp, L. W.; Lin, S. J.; Yuan, D. S.; Klausner, R. D.; Culotta, V. C.; Gitlin, J. D. *J. Biol. Chem.* **1997**, *272*, 9221.
- Hung, I. H.; Casareno, R. L.; Labesse, G.; Mathews, F. S.; Gitlin, J. D. *J. Biol. Chem.* **1998**, *273*, 1749.
- Terada, K.; Schilsky, M. L.; Miura, N.; Sugiyama, T. *Int. J. Biochem. Cell Biol.* **1998**, *30*, 1063.
- Arguello, J. M.; Eren, E.; Gonzalez-Guerrero, M. *Biometals* **2007**, *20*, 233.
- DiDonato, M.; Narindrasorasak, S.; Forbes, J. R.; Cox, D. W.; Sarkar, B. *J. Biol. Chem.* **1997**, *272*, 33279.
- Lutsenko, S.; Petrukhin, K.; Cooper, M. J.; Gilliam, C. T.; Kaplan, J. H. *J. Biol. Chem.* **1997**, *272*, 18939.
- Larin, D.; Mekios, C.; Das, K.; Ross, B.; Yang, A. S.; Gilliam, T. C. *J. Biol. Chem.* **1999**, *274*, 28497.
- Strausak, D.; Howie, M. K.; Firth, S. D.; Schlicksupp, A.; Pipkorn, R.; Multhaup, G.; Mercer, J. F. *J. Biol. Chem.* **2003**, *278*, 20821.
- van Dongen, E. M.; Klomp, L. W.; Merkx, M. *Biochem. Biophys. Res. Commun.* **2004**, *323*, 789.
- Walker, J. M.; Huster, D.; Ralle, M.; Morgan, C. T.; Blackburn, N. J.; Lutsenko, S. *J. Biol. Chem.* **2004**, *279*, 15376.
- Achila, D.; Banci, L.; Bertini, I.; Bunce, J.; Ciofi-Baffoni, S.; Huffman, D. L. *Proc. Natl. Acad. Sci. U.S.A.* **2006**, *103*, 5729.
- Banci, L.; Bertini, I.; Cantini, F.; Rosenzweig, A. C.; Yatsunyk, L. A. *Biochemistry* **2008**, *47*, 7423.
- Rodriguez-Granillo, A.; Crespo, A.; Wittung-Stafshede, P. *Biochemistry* **2009**, *48*, 5849.
- Banci, L.; Bertini, I.; Cantini, F.; Massagni, C.; Migliardi, M.; Rosato, A. *J. Biol. Chem.* **2009**, *284*, 9354.
- Lutsenko, S.; Leshane, E. S.; Shinde, U. *Arch. Biochem. Biophys.* **2007**, *463*, 134.
- Voskoboinik, I.; Mar, J.; Strausak, D.; Camakaris, J. *J. Biol. Chem.* **2001**, *276*, 28620.
- Tsvikovskii, R.; MacArthur, B. C.; Lutsenko, S. *J. Biol. Chem.* **2001**, *276*, 2234.
- DiDonato, M.; Hsu, H. F.; Narindrasorasak, S.; Que, L., Jr.; Sarkar, B. *Biochemistry* **2000**, *39*, 1890.
- Sali, A.; Blundell, T. L. *J. Mol. Biol.* **1993**, *234*, 779.
- Fiser, A.; Do, R. K.; Sali, A. *Protein Sci.* **2000**, *9*, 1753.
- Marti-Renom, M. A.; Stuart, A. C.; Fiser, A.; Sanchez, R.; Melo, F.; Sali, A. *Annu. Rev. Biophys. Biomol. Struct.* **2000**, *29*, 291.
- Eswar, N.; Webb, B.; Marti-Renom, M. A.; Madhusudhan, M. S.; Eramian, D.; Shen, M. Y.; Pieper, U.; Sali, A. *Current Protocols in Protein Science*; John Wiley & Sons, Inc., 2007; Chapter 2, Unit 2.9.
- Cornell, W. D.; Cieplak, P.; Bayly, C. I.; Gould, I. R.; Merz, K. M.; Ferguson, D. M.; Spellmeyer, D. C.; Fox, T.; Caldwell, J. W.; Kollman, P. A. *J. Am. Chem. Soc.* **1995**, *117*, 5179.
- Pearlman, D. A.; Case, D. A.; Caldwell, J. W.; Ross, W. S.; Cheatham, T. E., III; DeBolt, S.; Ferguson, D.; Seibel, G.; Kollman, P. *Comput. Phys. Commun.* **1995**, *91*, 1.
- Case, D. A.; Cheatham, T. E., III; Darden, T.; Gohlke, H.; Luo, R.; Merz, K. M., Jr.; Onufriev, A.; Simmerling, C.; Wang, B.; Woods, R. J. *J. Comput. Chem.* **2005**, *26*, 1668.
- Case, D. A.; Darden, T. A.; Cheatham, T. E., III; Simmerling, C. L.; Wang, J.; Duke, R. E.; Luo, R.; Merz, K. M.; Pearlman, D. A.; Crowley, M.; Walker, R. C.; Zhang, W.; Wang, B.; Hayik, S.; Roitberg, A.; Seabra, G.; Wong, K. F.; Paesani, F.; Wu, X.; Brozell, S.; Tsui, V.; Gohlke, H.; Yang, L.; Tan, C.; Mongan, J.; Hornak, V.; Cui, G.; Beroza, P.; Mathews, D. H.; Schafmeister, C.; Ross, W. S.; Kollman, P. A. *AMBER 9*; University of California: San Francisco, CA, 2006.
- Jorgensen, W. L.; Chandrasekhar, J.; Madura, J.; Impey, R. W.; Klein, M. L. *J. Chem. Phys.* **1983**, *79*, 926.
- Hornak, V.; Abel, R.; Okur, A.; Strockbine, B.; Roitberg, A.; Simmerling, C. *Proteins* **2006**, *65*, 712.
- Berendsen, H. J.; Postma, J. P.; van Gunsteren, W. F.; Di Nola, A.; Haak, J. R. *J. Chem. Phys.* **1984**, *81*, 3684.
- Ryckaert, J. P.; Ciccotti, G.; Berendsen, H. J. C. *J. Comput. Phys.* **1977**, *23*, 327.
- Karplus, M.; Ichiye, T. *J. Mol. Biol.* **1996**, *263*, 120.
- Naim, M.; Bhat, S.; Rankin, K. N.; Dennis, S.; Chowdhury, S. F.; Siddiqi, I.; Drabik, P.; Sulea, T.; Bayly, C. I.; Jakalian, A.; Purisima, E. O. *J. Chem. Inf. Model.* **2007**, *47*, 122.
- Cui, Q.; Sulea, T.; Schrag, J. D.; Munger, C.; Hung, M. N.; Naim, M.; Cygler, M.; Purisima, E. O. *J. Mol. Biol.* **2008**, *379*, 787.
- Chen, W.; Chang, C. E.; Gilson, M. K. *Biophys. J.* **2004**, *87*, 3035.
- Caca, K.; Ferenci, P.; Kuhn, H. J.; Polli, C.; Willgerodt, H.; Kunath, B.; Hermann, W.; Mossner, J.; Berr, F. *J. Hepatol.* **2001**, *35*, 575.
- Todorov, T.; Savov, A.; Jelev, H.; Pantelieva, E.; Konstantinova, D.; Krustev, Z.; Mihaylova, V.; Tournev, I.; Tankova, L.; Tzolova, N.; Kremensky, I. *Clin. Genet.* **2005**, *68*, 474.
- Gromadzka, G.; Schmidt, H. H.; Genschel, J.; Bochow, B.; Rodo, M.; Tarnacka, B.; Litwin, T.; Chabik, G.; Czonkowska, A. *Clin. Gen.* **2005**, *68*, 524.
- Ichiye, T.; Karplus, M. *Proteins* **1991**, *11*, 205.
- Falconi, M.; Altobelli, G.; Iovino, M. C.; Politi, V.; Desideria, A. *J. Comput.-Aided Mol. Des.* **2003**, *17*, 837.
- Cansu, S.; Doruker, P. *Biochemistry* **2008**, *47*, 1358.

- (43) Banci, L.; Bertini, I.; Cantini, F.; Della-Malva, N.; Migliardi, M.; Rosato, A. *J. Biol. Chem.* **2007**, *282*, 23140.
- (44) Banci, L.; Bertini, I.; Cantini, F.; Massagni, C.; Migliardi, M.; Rosato, A. *J. Biol. Chem.* **2009**, *284*, 9354.
- (45) Hussain, F.; Olson, J. S.; Wittung-Stafshede, P. *Proc. Natl. Acad. Sci. U.S.A.* **2008**, *105*, 11158.
- (46) Rodriguez-Granillo, A.; Wittung-Stafshede, P. *Biochemistry* **2009**, *48*, 960.
- (47) Rodriguez-Granillo, A.; Wittung-Stafshede, P. *J. Phys. Chem. B* **2009**, *113*, 1919.
- (48) Tsay, M. J.; Fatemi, N.; Narindrasorasak, S.; Forbes, J. R.; Sarkar, B. *Biochim. Biophys. Acta* **2004**, *1688*, 78.
- (49) Bartee, M. Y.; Ralle, M.; Lutsenko, S. *Biochemistry* **2009**, *48*, 5573.
- (50) Guo, Y.; Nyasae, L.; Braiterman, L. T.; Hubbard, A. L. *Am. J. Physiol. Gastrointest. Liver Physiol.* **2005**, *289*, G904.
- (51) Schaefer, M.; Hopkins, R. G.; Failla, M. L.; Gitlin, J. D. *Am. J. Physiol.* **1999**, *276*, G639.
- (52) Sharma, S.; Rosato, A. *J. Chem. Inf. Model.* **2009**, *49*, 76.

JP909450X